JOURNAL OF AIRCRAFT
Vol. 35, No. 3, May–June 1998

Aeroelastic Analysis of Transient Blade Dynamics During Shipboard Engage/Disengage Operations

William P. Geyer Jr.*
U.S. Naval Air Warfare Center, Patuxent River, Maryland 20670-5304
and
Edward C. Smith† and Jonathan A. Keller‡
Pennsylvania State University, University Park, Pennsylvania 16802-1401

An analysis has been developed to predict transient aeroelastic rotor response during shipboard engage/disengage sequences. The blade is modeled as an elastic beam undergoing deflections in flap and torsion. The blade equations of motion are formulated using Hamilton's principle and they are spatially discretized using the finite element method. The discretized blade equations of motion are integrated for a specified rotor speed run-up or run-down profile. Blade element theory is used to calculate quasisteady or unsteady aerodynamic loads in linear and nonlinear regimes. Three different simple wind-gust distributions are modeled. Basic ship-roll motion characteristics are also included in the shipboard airwake environment. An H-46 rotor system model is developed and shows excellent correlation with experimental static tip deflection and blade natural frequency data. Parametric studies are conducted to systematically investigate the effects of collective and cyclic pitch control settings, droop stop angle, and ship motion on blade response. These studies indicate that collective and cyclic control inputs have a moderate effect on maximum negative tip deflections. Torsion is shown not to be required for rotorcraft with small amounts of pitch–flap coupling. Unsteady aerodynamics is shown only to be important to the blade response at high wind speeds for spatially varying gusts. A flap damper is incorporated and is effective in reducing tip deflections if the flap stop angle is increased.

Nomenclature

C = damping matrix
C_β = flap damper strength
h_{cg} = height of rotor disk above ship c.g.
$\hat{\boldsymbol{I}}_H, \hat{\boldsymbol{J}}_H, \hat{\boldsymbol{K}}_H$ = unit vectors in hub coordinate system
K = stiffness matrix
K_β = droop/flap stop spring stiffness
M = mass matrix
P = ship-roll period
$\boldsymbol{Q}$ = load vector
$\boldsymbol{q}$ = global vector of nodal displacements
T = kinetic energy of blade
t = time
t_i = initial time
t_f = final time
U = total potential energy of blade
U_B = potential (strain) energy of blade
U_{DS} = potential energy of droop stop
U_{FS} = potential energy of flap stop
U_{PL} = potential energy of pitch link
$\boldsymbol{V}^{gust}$ = velocity vector of blade relative to airflow
V_{roll} = lateral wind speed caused by ship-roll motion
V_{wod} = relative wind-over-deck speed
V_{vert} = vertical wind speed
V_x^{gust} = longitudinal wind speed
V_y^{gust} = lateral wind speed
V_z^{gust} = vertical wind speed
W = total work done by external forces
W_{AF} = work done by aerodynamics forces
W_{FD} = work done by flap damper
W_G = work done by gravitational forces
w'_{DS} = droop stop angle
x = nondimensional radial location along blade
α_w = angle of wind-over-deck above horizon
$\Delta w'$ = flap hinge angle
δ = variational operator
κ_{lat} = deterministic gust lateral scaling component
κ_{vert} = deterministic gust vertical scaling component
Π = total energy
Φ_c = modal matrix of cantilevered mode shapes
Φ_h = modal matrix of hinged mode shapes
ϕ_{max} = maximum ship-roll angle
ϕ_s = ship-roll angle
ψ = rotor blade azimuthal angle
$\bar{\psi}$ = nondimensional time
ψ_{wod} = relative wind-over-deck direction
Ω = rotor rotational speed
Ω_{DS} = rotor rotational speed when droop/flap stops extend/retract
Ω_0 = reference rotor rotational speed

Subscripts
a = inboard node of element
b = outboard node of element
i = ith finite element

Superscripts
$\dot{}$ = $\partial(\ )/\partial t$
$\ddot{}$ = $\partial^2(\ )/\partial t^2$

Received Feb. 6, 1997; revision received Oct. 1, 1997; accepted for publication Oct. 10, 1997. This paper is declared a work of the U.S. Government and is not subject to copyright protection in the United States.

*Flight Test Engineer, Aircraft Division, Test and Evaluation Engineering Department. Member AIAA.
†Assistant Professor, Department of Aerospace Engineering. Member AIAA.
‡Graduate Research Assistant, Department of Aerospace Engineering. Student Member AIAA.

Introduction

SINCE 1943, the U.S. Navy has operated rotorcraft aboard ships, where unique and often hazardous conditions can

be encountered. One potential problem can occur during the engagement and disengagement of the rotor system while the helicopter is on the flight deck. Excessive aeroelastic flapping of the rotor blades can occur at low rotor speeds, when the centrifugal stiffening is low, because of high winds and sea states. In some conditions, the blade's flapping becomes large enough for it to contact the helicopter's fuselage, resulting in a tunnel strike for tandem rotor configurations (Fig. 1), or the tailboom, resulting in a tailboom strike for single-rotor configurations. The H-46 Sea Knight, a tandem rotor helicopter used by the U.S. Navy and Marines, has encountered over 100 tunnel strikes since 1964 and still occasionally experiences them. Most tunnel strikes cause minor damage such as denting or tearing the synchronization shaft cover or cracking the synchronization shaft mounts. Major damage involves severing the synchronization shaft, blade failure, or droop stop failure. The U.S. Navy has conducted several shipboard H-46 engage/disengage tests and has determined that shipboard testing is too costly and time consuming because of the large number of variables involved; but analytical methods to predict the tunnel strike event are currently being explored.

In 1985, tailboom strikes were investigated using a flapwise elastic rotor code of a hingeless rotor system.[1] The transient blade response was predicted using analytic run-up and run-down rotor speed time histories and quasisteady aerodynamics, including a Kirchoff trailing-edge separation model. The ship airwake environment included ship-roll motion effects on wind and simple deterministic gusts that were developed from model scale wind-tunnel surveys correlated with full-scale ship airwake data. The aerodynamic model was later improved by including flap–torsion coupling and the deterministic gust model was correlated with additional wind-tunnel experiments.[2] In 1992, the elastic flap code was modified to model articulated (hinged) rotor systems in which blade motion is constrained from excessive upward and downward flapping motion by mechanical flap and droop stops.[3] These stops were modeled using high-rate linear springs that apply a restraining force only when the blade flap deflection at the spring location is large enough to cause contact. Recent studies were conducted to validate the rotor analysis in which a model rotor system with rigid, teetering blades was placed aboard a scaled ship deck and tested in a wind tunnel.[4,5] The influence of the ship's structure was proven to be very important to the blade's behavior and the largest flap deflections occurred for the hub location one-quarter of the deck's width from the windward deck edge.

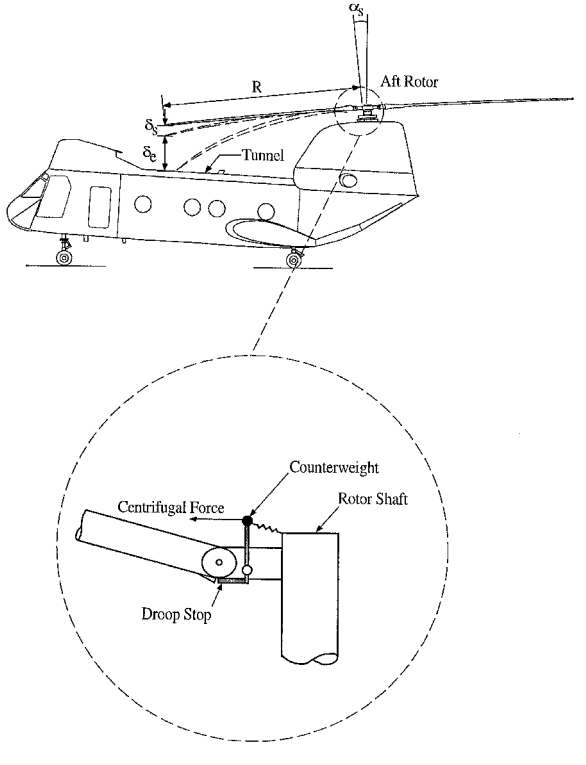

Fig. 1 H-46 and droop stop schematic.

The objective of the current research is to develop an alternative and improved analysis, compared to Refs. 1–5, capable of predicting transient blade response during shipboard engage/disengage operations. The present research differs from earlier efforts in several ways. Flap–torsion elastic blade motions are predicted using the finite element method (FEM) to provide for greater flexibility in modeling different hub types. A time-domain unsteady aerodynamic model based on indicial response is used to calculate airloads in the attached flow, nonlinear separation, and dynamic stall regimes. Experimentally measured H-46 run-up/run-down rotor speed time histories are employed in the prediction of the transient blade response. Using this analysis, an H-46 blade model is developed and validated against experimental data. Parametric studies are conducted to systematically investigate the effects of collective and cyclic control settings, droop stop angle, and ship motion on blade response. A preliminary study of the effectiveness of a flap damper in reducing tip deflections is conducted. Furthermore, the importance of torsion and unsteady aerodynamics to the simulation of the blade response is determined.

Helicopter Model

The blade strike analysis differs from most rotorcraft analyses because the blade strike phenomenon occurs under low-thrust and low-rotor speed conditions. The rotor speed run-up/run-down profiles are functions of time and are rotorcraft specific. An important issue when performing a transient analysis is the difference between ψ and $\bar{\psi}$. These terms are considered the same when integrating the blade equations of motion for a constant rotor speed equal to Ω_o. For this analysis, ψ and $\bar{\psi}$, given in radians, are defined as

$$\psi = \int_0^{t_f} \Omega(t)\, dt \tag{1a}$$

$$\bar{\psi} = \Omega_o t \tag{1b}$$

Blade flap and torsional deflections are predicted using the Bernoulli–Euler beam bending theory. Radial variations in elastic, inertial, and aerodynamic properties are accommodated by employing the FEM. The assumptions in this analysis include the following: the total rotor thrust is close to zero, which precludes the need for inflow and ground-effect models; gravity forces are necessary because the blade operates at low rotor speeds; ship motion effects on blade inertial loads are negligible because of low ship motion frequencies relative to the rotor frequency[2]; and lead–lag degrees of freedom are neglected because the portion of the engage/disengage sequence in which the majority of tunnel strikes occur is where $\Omega(t)$ is less than 20% of Ω_o.[6] In this region coriolis forces are small. Also, most articulated rotor blades have small amounts of twist, which reduces flap–lag coupling.

Formulation Using Hamilton's Principle

The partial differential equations governing blade motion are derived using the generalized Hamilton's principle:

$$\delta\Pi = \int_{t_i}^{t_f} (\delta T - \delta U + \delta W)\, dt = 0 \tag{2}$$

Detailed formulations of all terms are presented in Refs. 7 and 8. The variation of strain energy and virtual work are com-

posed of aerodynamic forces, gravity forces, pitch link stiffness, and droop stop stiffness and are expressed as follows:

$$\delta U = \delta U_B + \delta U_{DS} + \delta U_{PL} + \delta U_{FS} \quad (3)$$

$$\delta W = \delta W_G + \delta W_{AF} + \delta W_{FD} \quad (4)$$

Brief formulations of the variation of droop and flap stop strain energy and flap damping are presented next.

The rotor system features most important to the engage/disengage process for an articulated rotor system are the droop and flap stops. The droop stop, shown in Fig. 1, restrains the downward rotation of the flap hinge during low rotor speeds and at rest. The flap stop restrains upward flap hinge motion using the same type of mechanism. The position of the droop stop (extended/retracted) is governed by the pulling of centrifugal force on a counterweight acting against a spring force. When the centrifugal force pulling on the counterweight is less than the spring force, the droop stop extends, as shown in Fig. 1, and the mechanism restrains the flap hinge from rotating past the droop stop angle. When the centrifugal force pulling on the counterweight is greater than the spring force, the droop stop rotates downward (retracts), which enables the blade to flap freely. In the analysis, the position of the droop stop during rotor engage/disengage is determined by Ω_{DS}.

The droop and flap stop interactions with the blade are modeled using a conditional rotational spring located at the flap hinge. While the droop stop is extended, the rotational spring stiffness is zero for hinge angles greater than the droop stop angle and large enough ($K_\beta = 2.84 \times 10^7$ ft-lb/rad) to restrict the flap hinge rotation to less than 0.1 deg for hinge angles equal to or below the droop stop angle. The strain energy for the droop stop is expressed as

$$U_{DS} = \tfrac{1}{2} K_\beta (\Delta w' - w'_{DS})^2 \quad (5)$$

Taking the variation of this strain energy expression, the equation becomes

$$\delta U_{DS} = K_\beta (\Delta w' - w'_{DS}) \delta \Delta w' \quad (6)$$

In addition, two situations must be modeled to ensure proper physical behavior of the droop stop. During rotor engagement, the blade may be in contact with the droop stop upon reaching Ω_{DS}; however, the droop stop cannot retract until the blade lifts off of it. During rotor disengagement, the blade may be flapped below the droop stop angle upon reaching Ω_{DS}; however, the droop stop cannot extend until the blade flaps above the droop stop angle. In a similar manner, these situations also exist for the flap stop.

Reference 9 indicates that under certain wind conditions the blade violently strikes the droop stop, causing a transfer of system energy from kinetic to potential (strain). Preliminary rotor engage simulations are performed investigating the possibility of reducing the blade deflection by adding a rotational damper acting at the flap hinge. Flap dampers have been used on early shipborne helicopters such as the HUP-1 through HUP-4 series to reduce excessive blade flapping during low-rotor speed operation,[10] but are not in use on the H-46. The flap damper is assumed to extend/retract at the same rotor speed as the droop and flap stops and to act through the entire angular range between the droop and flap stops. The virtual work performed on the blade because of the flap damper is

$$\delta W_{FD} = -C_\beta \Delta w' \delta \Delta w' \quad (7)$$

Aerodynamic Modeling

The shipboard aerodynamic environment consists of ship-roll motion effects on ambient winds and deterministic gust distributions over the rotor disk. The ship is assumed to be stationary with respect to the inertial coordinate system, except for roll motion. The atmospheric winds relative to the ship are uniform and are termed the relative wind-over-deck (WOD) conditions defined by V_{wod}, ψ_{wod}, and V_{vert} (Fig. 2).

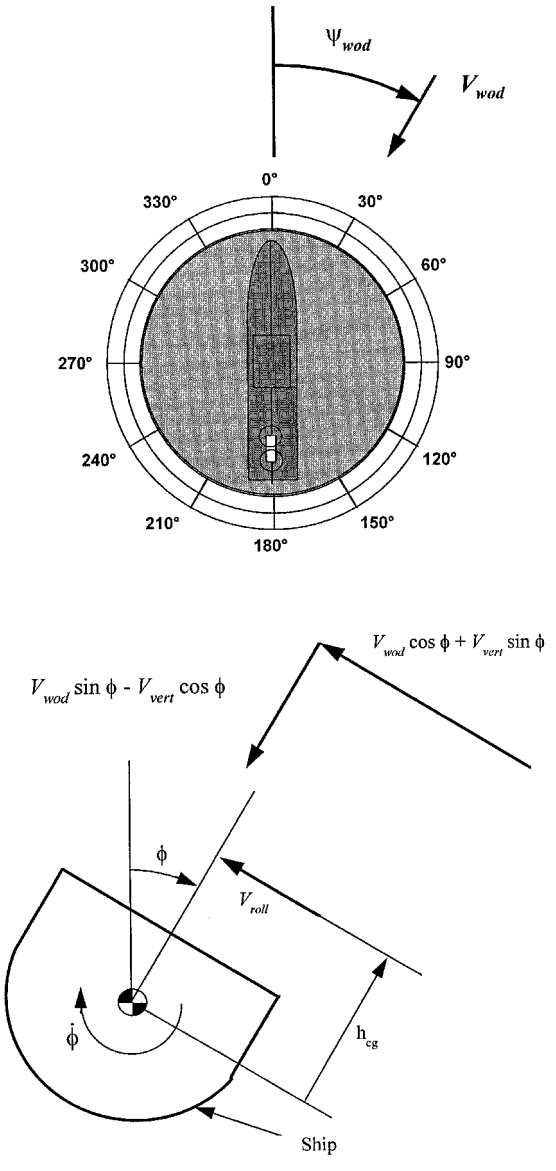

Fig. 2 Analytic model of shipboard aerodynamic environment.

Recall that ship motion effects on blade inertia forces were assumed negligible; however, ship motion effects on blade airloads are included. Typical amplitudes and frequencies of the six ship motions (surge, sway, heave, pitch, roll, and yaw) are provided in Ref. 11. In higher sea states, pitch and roll motions are indicated to be more dominant. The present research models ship-roll motion to remain consistent with Refs. 1–3. The ship-roll motion aerodynamic model consists of the transformed relative WOD conditions caused by the ship-roll angle and a wind component at the hub height caused by the angular-roll velocity (Fig. 2). Ship-roll motion is governed by sinusoidal variation of ϕ_s and can be expressed as

$$\phi_s = \phi_{max} \sin(2\pi \bar{\psi}/P) \quad (8)$$

The roll angular velocity causes a lateral wind velocity at the hub height given by

$$V_{roll} = \phi_{max} h_{cg} (2\pi/P) \cos(2\pi \bar{\psi}/P) \quad (9)$$

Two gust models that simulate the airflow over a ship's flight deck subjected to a crosswind are explored in this analysis. The first model, the linear gust developed in Ref. 2, is adopted to explore the local wind variations over the rotor disk on the blade response. This gust consists of an upward wind component on the windward half of the rotor disk transitioning linearly to a downward wind component on the leeward half of the disk. The second model, the uniform gust detailed in Ref. 7, is used to determine the effects of uniform vertical winds on the blade response. This gust consists of a uniform downward velocity across the rotor disk. In addition, each model features a lateral wind component in the direction of the relative WOD velocity. The wind velocity resulting from either gust model can be expressed as

$$\boldsymbol{V}^{\text{gust}} = \boldsymbol{V}_x^{\text{gust}}\hat{\boldsymbol{I}}_H + \boldsymbol{V}_y^{\text{gust}}\hat{\boldsymbol{J}}_H + \boldsymbol{V}_z^{\text{gust}}\hat{\boldsymbol{K}}_H \tag{10}$$

In the linear gust distribution the individual components are defined as

$$\boldsymbol{V}_x^{\text{gust}} = V_{\text{wod}}\kappa_{\text{lat}}\cos(\psi_{\text{wod}}) \tag{11a}$$

$$\boldsymbol{V}_y^{\text{gust}} = -V_{\text{wod}}\kappa_{\text{lat}}\sin(\psi_{\text{wod}}) \tag{11b}$$

$$\boldsymbol{V}_z^{\text{gust}} = V_{\text{wod}}\kappa_{\text{vert}}x\cos(\psi - \pi + \psi_{\text{wod}}) \tag{11c}$$

In the uniform gust distribution the individual components are defined as

$$\boldsymbol{V}_x^{\text{gust}} = V_{\text{wod}}\cos(\alpha_w)\cos(\psi_{\text{wod}}) \tag{12a}$$

$$\boldsymbol{V}_y^{\text{gust}} = -V_{\text{wod}}\cos(\alpha_w)\sin(\psi_{\text{wod}}) \tag{12b}$$

$$\boldsymbol{V}_z^{\text{gust}} = -V_{\text{wod}}\sin(\alpha_w) \tag{12c}$$

This analysis is able to predict both quasisteady and unsteady aerodynamic loads and allows many different levels of aerodynamic fidelity. The quasisteady aerodynamics development follows an unsteady thin airfoil theory development by Johnson.[12] This development includes the airloads caused from virtual mass (noncirculatory) effects and allows for either linear or nonlinear predictions using Kirchhoff's nonlinear separation model. The unsteady aerodynamic model used in this analysis was developed by Leishman and Beddoes.[13–15] This time-domain approach includes attached flow, unsteady trailing-edge separation, and dynamic stall effects. The attached flow, unsteady model is based on an indicial response formulation and predicts both circulatory and noncirculatory airloads. The unsteady trailing-edge separation model accounts for trailing-edge separation, leading-edge pressure lags, and unsteady boundary-layer effects. The dynamic stall model calculates the additional lift and large downward pitching moment created by the shedding vortex. Detailed descriptions of the incorporation of both aerodynamic models into the present analysis are given in Ref. 7.

Discretized Blade Equations of Motion

The generalized Hamilton's principle, Eq. (2), is used to formulate the blade equations of motion and the FEM is used to discretize them. Each flexible element has seven degrees of freedom and is cubic in flap bending and quadratic in torsion. The energy expressions are spatially discretized by substituting shape functions into the elemental virtual energy expressions and integrated in space using a six-point Gaussian quadrature method. The elemental mass, damping, stiffness matrices, and load vector are then assembled to form their global counterparts. The global discretized equation of motion becomes

$$M\ddot{\boldsymbol{q}} + C\boldsymbol{q} + K\boldsymbol{q} = \boldsymbol{Q} \tag{13}$$

The variations in strain energy for droop and flap stop stiffnesses are in terms of discrete degrees of freedom that have not been defined to this point. The flap hinge angle can be expressed as the difference between elemental degrees of freedom. The variation of strain energy because of droop stop stiffness, Eq. (6), becomes

$$\begin{aligned}\delta U_{\text{DS}} = {} & \delta(w_a')_i K_\beta[(w_a')_i - (w_b')_{i-1} - w_{\text{DS}}'] \\ & - \delta(w_b')_{i-1} K_\beta[(w_a')_i - (w_b')_{i-1} - w_{\text{DS}}']\end{aligned} \tag{14}$$

The expression for the variation in strain energy for flap stop stiffness is very similar to the one for the droop stop. The motion dependent terms are added to K and the motion independent terms are added to $\boldsymbol{Q}$.

Analysis

In the previous section, the theory used to model the blade structure and aerodynamic loads was discussed and the method used to discretize the blade equations of motion was described. Using these equations, three analyses, 1) an eigenanalysis, 2) a transient response analysis, and 3) an engage/disengage envelope analysis can be performed. These analyses are interdependent because the eigenanalysis is required for the transient response analysis and the transient response analysis is used in the engage/disengage envelope analysis. An eigenanalysis is used to determine the blade natural frequencies and mode shapes, and the engage/disengage envelope analysis is a tool used to determine the wind conditions for safe engage/disengage sequences.

The blade transient response is calculated by integrating the discretized blade equations of motion. Recall that the rotor speed and blade azimuth are functions of time and are used in the calculations of M, C, K, and $\boldsymbol{Q}$, which must be recalculated at every time step. The time integration is performed by a fourth-order Runge–Kutta scheme. The blade static deflection is used as the initial conditions for rotor run-up solutions. The steady-state response at the operational rotor speed is used as initial conditions for run-down solutions. Blade response can be computed in either physical or modal space, but modal space is recommended for computational efficiency.

Recall that a very stiff rotational spring is added to K to freeze the hinge angle during blade contact with either the droop or flap stop. Blade deflection during droop/flap stop contact is caused purely by elastic deformation with no rigid body rotation at the hinge. Once the blade lifts/drops off the droop/flap stop, the rotational spring is removed from K. An articulated rotor blade behaves in two distinct manners. When the blade is in contact with the droop/flap stop, it behaves like a cantilevered beam. When the blade is not in contact with the droop/flap stop, it behaves like a hinged beam. Before a time-integration begins, an eigenanalysis is performed to determine the hinged and cantilevered modes of the blade. Two techniques can be used to integrate the equations of motion in modal space. In the first method, called modal swapping off, only the hinged modes are used regardless of whether the blade is in contact with the droop/flap stop

$$\Phi = \Phi_h \quad \text{if} \quad \Delta w' > w_{\text{DS}}' \qquad \Phi = \Phi_h \quad \text{if} \quad \Delta w' \le w_{\text{DS}}' \tag{15}$$

More hinged modes are required to approximate the blade response because they do not represent the purely elastic deformation that occurs during a droop/flap stop contact. In the second method called modal swapping on, the appropriate set of modes, either cantilevered or hinged, is used depending on whether the blade is or is not in contact with the droop/flap stop

$$\Phi = \Phi_h \quad \text{if} \quad \Delta w' > w_{\text{DS}}' \qquad \Phi = \Phi_c \quad \text{if} \quad \Delta w' \le w_{\text{DS}}' \tag{16}$$

Fewer modes are required to approximate the blade response, because the appropriate set of modes is always used. This method also leads to the use of a larger time step.

Convergence studies are performed for a simulated H-46 rotor engagement to determine the lowest number of modes and the largest time step necessary for an accurate solution. The convergence study performed on the effects of time step gives an indication of the time savings the modal swapping on technique can provide. A converged solution performed in physical space, with 69 degrees of freedom and a maximum time step of 1 μs, required 105 h of CPU time. The same simulation was performed in modal space and generated using six modes (five flap and one torsion). Using the modal swapping off technique, a converged solution was generated with a maximum time step of 10 μs and required only 2.4 h of CPU time. Finally, using the modal swapping on technique, a converged solution was generated with a maximum time step of 100 μs and required only 15 min of CPU time. This illustrates the savings in time gained by employing the modal swapping on technqiue.

H-46 Blade Model Validation

The H-46 Sea Knight is a three-bladed tandem rotor helicopter, but the present research only models a single rotor blade of the aft rotor system, using 12 finite elements. Further details of the H-46 blade finite element model are presented in Ref. 7. The droop and flap stop angles are −0.54 and 1.5 deg, respectively. During all rotor engage/disengage sequences, the collective is 3 deg, the longitudinal cyclic is 2.5 deg, and the lateral cyclic is 0.0693 deg. These control inputs are termed the standard control inputs and are derived from the auto cyclic trim settings used in actual H-46 operations. The standard control inputs are used for all parametric studies unless otherwise noted.

Proper stiffness and mass distributions are verified by comparing the predicted static tip deflection under the blade's weight to experimental data. Reference 8 provides the static tip deflection data of the blade clamped at the two-pin retention and provides the same results from the FEM. The predicted static tip deflection of 15.3 in. is within 2.6% of the Boeing test data average. A fan diagram is also developed to determine how well the finite element approach models the H-46 flap and torsion rotating natural frequencies. Figure 3 illustrates the first four coupled flap–torsion frequencies overlaid with test data for the second through the fourth flap modes from Ref. 7. The flap–torsion elastic analysis is in satisfactory agreement with the blade data.

Parametric Studies

Typical Rotor Engagement and Disengagement

A typical rotor engagement and disengagement were simulated using a linear gust model, with V_{wod} = 40 kn, κ_{vert} = 25%, and ψ_{wod} = 90 deg. The experimentally measured H-46 run-up rotor and run-down rotor speed profiles with a rotor brake application at 55% of Ω_o, both developed in Ref. 9, are used in this analysis. Representative blade responses using these rotor speed profiles are shown in Fig. 4. Note for rotor engagement, the tip deflections decrease as the rotor speed increases, and the maximum downward tip deflection occurs at approximately 7 s into the engagement. During rotor disengagement, the blade deflections steadily grow. Note that when the rotor brake is applied, the tip deflections grow more rapidly and the maximum deflection occurs within the last 2 s.

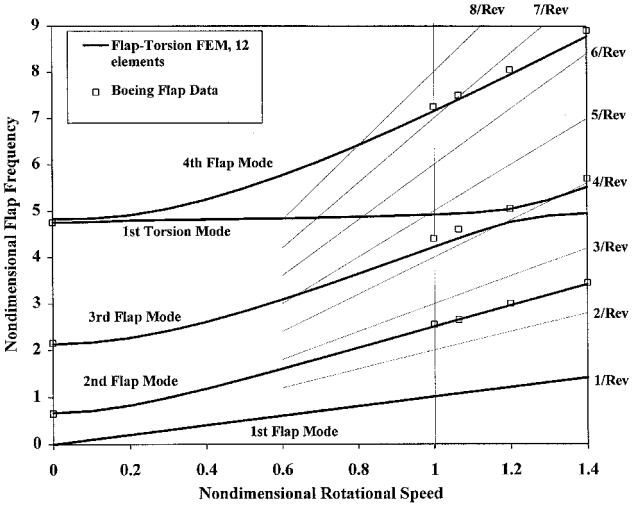

Fig. 3 H-46 blade fan diagram.

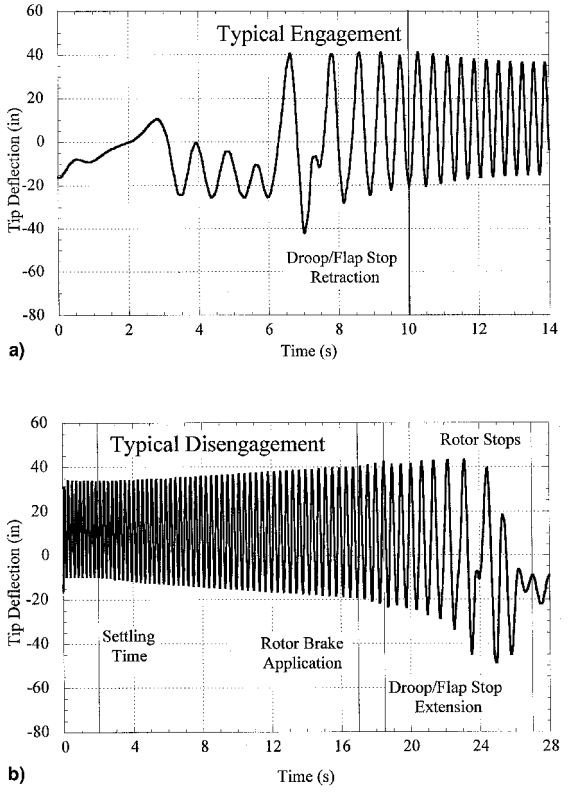

Fig. 4 Typical transient blade response for rotor: a) engagement and b) disengagement.

Gust Model Effects

The effects of a uniform gust and a linearly distributed gust on the H-46 blade response during a rotor engagement are examined. Both gusts consist of V_{wod} = 40 kn and approach from ψ_{wod} = 90 deg. For the uniform gust α_w = 15 deg, whereas for the linear gust κ_{vert} = 25%. The resulting tip and flap hinge angle responses are shown in Fig. 5. Note that for the uniform gust, the aerodynamic forces cause the blade to reach its maximum downward tip deflection almost immediately. In contrast, the blade response for the linear gust involves substantial blade/droop stop interaction. Note that while the droop stop is initially extended, the blade rises above the hub and then violently strikes the droop stop. The sudden halt of the flap hinge rotation indicates a transfer of system energy from kinetic to potential (strain).

Importance of Torsion and Unsteady Aerodynamics

The purpose of this study is to determine whether higher fidelity models are required for accurate predictions of the tunnel strike phenomenon. Both flap and flap–torsion structural models are examined. For each structural model, both a nonlinear quasisteady aerodynamic model and a nonlinear unsteady with dynamic stall aerodynamic model are utilized. Negligible differences in the maximum tip deflection between both the aerodynamic and structural models were found using

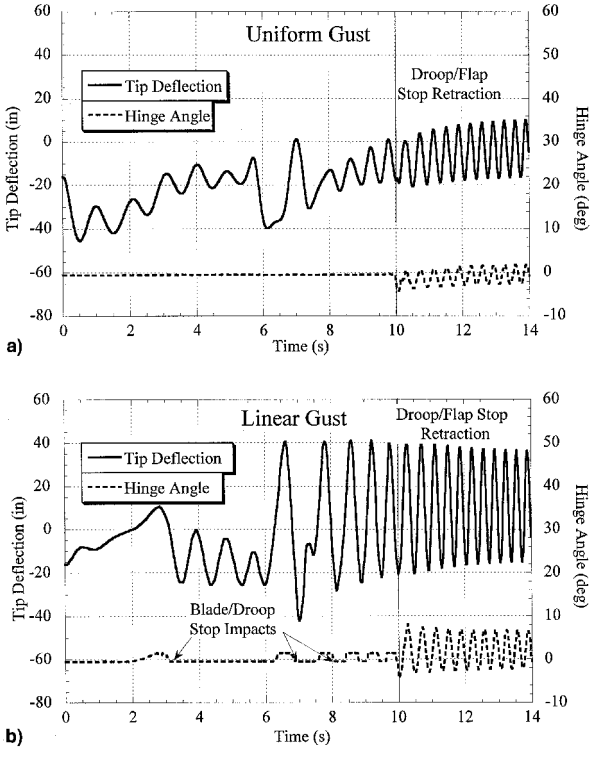

Fig. 5 Comparison of blade response characteristics for rotor engagement in a) uniform and b) linear gusts.

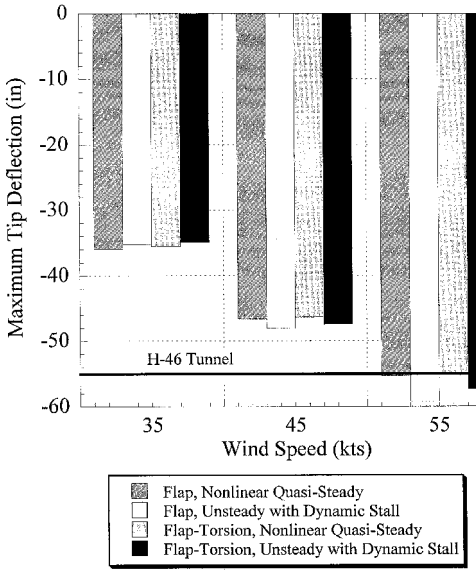

Fig. 6 Comparison of structural and aerodynamic models for rotor engagement in a linearly distributed gust.

the uniform gust model.[7] Differences were found for the linear gust model, and so the WOD conditions shown in this study are a linear gust model with V_{wod} = 35, 45, and 55 kn, κ_{vert} = 25%, and ψ_{wod} = 90 deg.

The results for the run-up case using the linearly distributed gust model are shown in Fig. 6. Similar to the blade response for the uniform gust, there are negligible differences between both the aerodynamic and structural models at 35 and 45 kn, but at 55 kn the differences in maximum downward tip deflection between the aerodynamic models become more pronounced. This study suggests that torsion is not required for the uniform or linearly distributed gusts; however, a higher fidelity aerodynamic model may be required for spatially varying gusts at higher wind speeds.

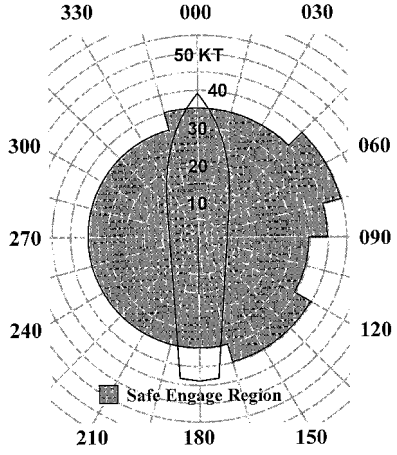

Fig. 7 H-46 safe engage envelope with standard control inputs.

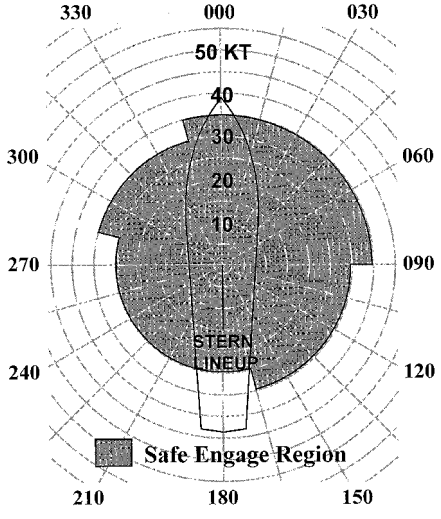

Fig. 8 H-46 safe engage envelope with standard control inputs −2-deg collective pitch.

Engage Envelope Study

The engage/disengage wind envelope analysis is used to determine the engage envelopes for this study. This analysis determines the blade-to-fuselage clearance for multiple wind-over-deck conditions using the maximum downward tip deflection calculated from the blade transient response. The safe engage region is composed of all wind-over-deck conditions with blade-to-fuselage clearances greater than 8 in.

An H-46 baseline engagement envelope developed using standard control inputs and a uniformly distributed gust with α_w = 15 deg is shown in Fig. 7. Note that the H-46 is limited to wind speeds of 30 kn for port WOD conditions and is limited to 35 kn for most starboard WOD conditions. The predicted envelope shows safe engagements for wind speeds up to 40 kn for WOD directions of 45− 75 deg. Results of sensitivity studies performed in Ref. 7 showed that control inputs have a moderate effect on maximum downward tip deflections. The two following studies show the effect of 2-deg variations in collective and cyclic path controls from the standard control inputs.

The predicted H-46 engage envelope for a collective pitch decrease of 2 deg from standard control inputs is shown in Fig. 8. A comparison with the baseline engagement envelope shows a 5-kn reduction in the safe engagement region for WOD directions of 45−75 deg and 120−285 deg. This results in a 14.5% reduction in the H-46 engagement capability. The predicted H-46 engage envelope for a lateral cyclic pitch increase of 2 deg from standard control inputs is shown in Fig.

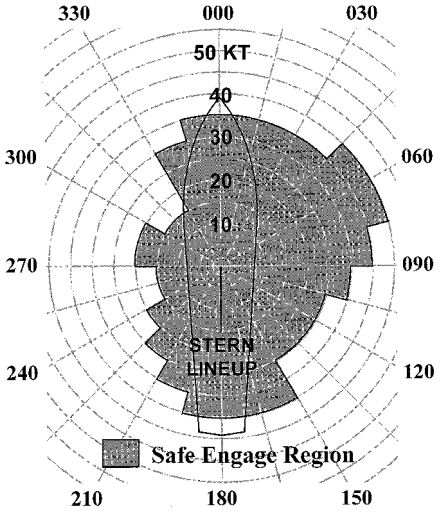

Fig. 9 H-46 safe engage envelope with standard control inputs +2-deg lateral cyclic.

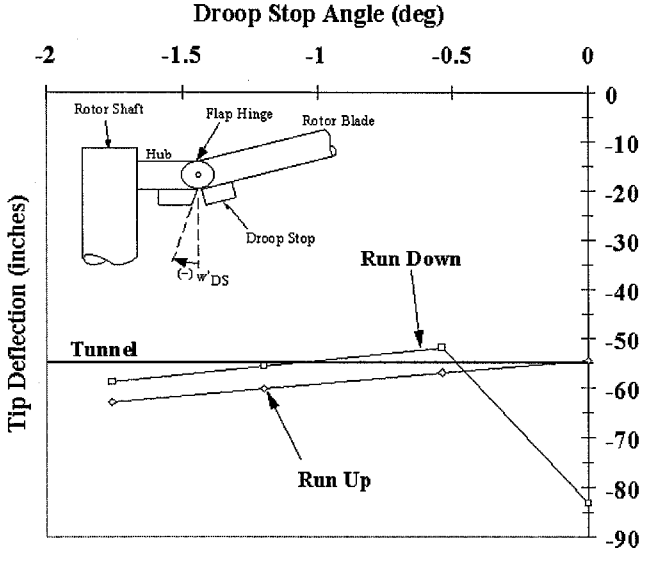

Fig. 10 Droop stop angle effects on maximum downward tip deflections

9. Unlike the small decrease in wind speed over large portions of the envelope for the collective pitch change, note the substantial reduction in engagement capability for port winds. WOD speeds are reduced by 10–15 kn for WOD directions from 120–150 deg and from 225–330 deg. There was a small 5-kn increase in the safe engage region for stern winds from 165 to 195 deg. This results in a 20.7% reduction in the safe-engage region. These results illustrate that during engagements in uniformly distributed winds, small changes in collective and cyclic inputs can moderately effect the safe-engage region.

Droop Stop Angle Effects

It is obvious that decreasing the droop stop angle decreases the static blade/fuselage clearance; however, the effects on the dynamic response of the blade are more uncertain. Figure 10 shows the effects of droop stop angle variation on maximum negative tip deflection. In this study, the droop stop was increased from −1.25 to 0 deg. Note that for the run-up case, an increase in droop stop angle decreases the maximum tip deflection. The run-down case deviates from this trend for the 0-deg droop stop angle position. In this case, the blade did not flap upward sufficiently enough for the droop stop to extend. The effectiveness of droop stop rotation on the maximum negative tip deflection is not very large for this WOD conditions. Further studies of blade response to droop stop angle variation are recommended for other WOD conditions. But this initial study does not suggest that droop stop angle changes would be an effective means to controlling the tunnel strike phenomenon caused by the delay in droop stop extension at higher droop stop angles.

Flap Damping Study

In an effort to reduce the frequency of tunnel-strike occurrences, a preliminary investigation was conducted into the effectiveness of adding a rotational damper acting at the flap hinge of the H-46 to dissipate energy in the flapping degree of freedom. Rotor engagements were simulated for a linear gust with V_{wod} = 55 kn, κ_{vert} = 25%, and ψ_{wod} = 90 deg. Preliminary results for the current H-46 flap and droop stop settings, of −.54 and 1.5 deg, respectively, indicated that the flap damper, regardless of its strength, was not effective in reducing the blade deflection because the angular range of motion was too small. At very large damper strengths, the flap damper simply freezes the flap hinge angle because the energy necessary to rotate the highly damped hinge is much higher than the energy necessary to deform the blade. Raising the flap stop angle permits the damper to act through a larger angular range of motion and dissipate more energy. Combinations of flap stop settings from 1.5 to 10 deg and flap damper strengths ranging from zero to five times the H-46's lead/lag damper strength, or 17,500 ft-lb/(rad/s), were investigated as means of reducing the blade deflection.

The variation of the maximum negative tip deflection during each simulated engagement is shown in Fig. 11. Note with no flap damper a tunnel stike is predicted for every flap stop setting. At the current H-46 flap stop setting, the strongest damper reduces the maximum negative tip deflection by only 5.8 in. As the flap stop settings are raised and the flap damping increased, the maximum negative tip deflections decrease. For flap dampers greater than four times the lead/lag damper strength, the tip deflections increased because the blade was prevented from flapping up at the beginning of the rotor engagement.

Tip deflection time histories for rotor engagement are presented in Fig. 12. Two flap stop settings and flap damper combinations are examined. The flapping behavior of the rotor blade becomes excessive at both 2 and 6 s into the engagement because it is both rotating into the WOD and experiencing a strong upflow from the specified gust distribution. The maximum negative tip deflection occurred 7 s after engagement in both configurations. For a flap damper four times the strength of the lead/lag damper and a flap stop setting of 10 deg,

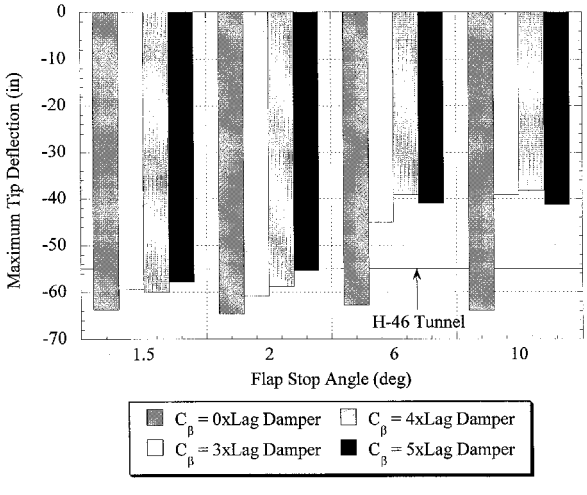

Fig. 11 Flap damping effects on the maximum downward tip deflection for various flap stop angles.

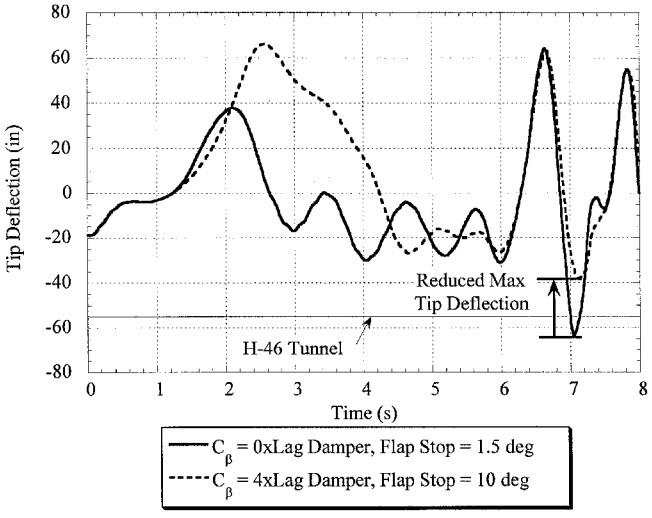

Fig. 12 Comparison of tip deflection time histories with and without flap damping.

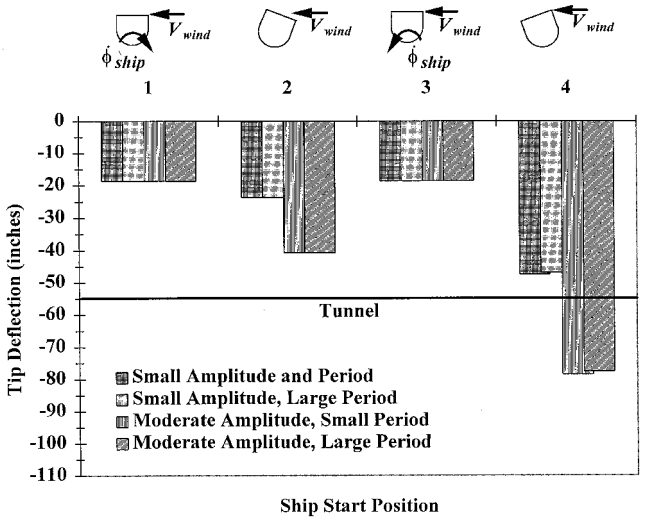

Fig. 13 Ship-motion effects on maximum tip deflection for rotor engagement.

enough energy is dissipated to prevent a tunnel strike in this simulation.

In summary, a tradeoff exists between flap damping and flap stop setting. With a low flap stop setting, the blade does not develop excessive potential energy because of excessive flapping; however, the flap damper cannot dissipate much energy when acting through such a small angle. At higher flap stop settings, the blade is allowed to develop extra potential energy from increased flapping that is transferred to strain energy upon droop stop contact; but the flap damper can dissipate more energy because it acts through a larger angle. Substantial tip deflection reductions occur only when the energy the flap damper dissipates becomes greater than the potential energy developed by the blade in excessive flapping. For the current H-46 flap stop setting of 1.5 deg, this analysis suggests that the tip deflections cannot be substantially reduced using a flap damper. If the flap stop is raised and a flap damper four times the strength of the lead/lag damper is employed, reductions of 40% of the maximum negative tip deflection can result.

Ship Motion Effects

Several H-46 rotor engagements were simulated for combinations of ship-roll period, maximum roll amplitude, and ship-roll starting position. The roll periods are 3 and 9 s and maximum roll amplitudes are 5 and 10 deg. The ship motion is fixed so that as the blade started during engagements, the ship would be at a specific point in its roll motion. Four specific cases of roll motion are included: the ship at the maximum starboard (case 2) and port (case 4) roll angles, and the ship passing through the zero angle rolling toward starboard (case 1) and port (case 3) directions.

The effects of ship motion on the maximum negative tip deflections for rotor engagement are shown in Fig. 13. Note for ship cases 1 and 3, the blade response is insensitive to changes in period and maximum amplitude. For ship cases 2 and 4, the blade response is large to changes in amplitude, which illustrates that it is very sensitive to the amount of inflow through the rotor disk. For the same ship positions, tip deflections are insensitive to the roll period. The insensitivity to roll period could be caused by the rotor speed profile. If the acceleration of the rotor system (dependent upon the rotor speed profile) is large compared to the ship motion, the blade does not feel the effects of the ship motion.

Conclusions

An analysis tool has been developed to predict transient aeroelastic rotor response during rotor engage/disengage sequences. This research is the first to address the effects of torsion and unsteady aerodynamics on the transient rotor response. In particular, this analysis is used to model the H-46 aft rotor system and parameters conducive to the tunnel-strike phenomenon are identified.

1) The predicted static tip deflection and natural frquencies in flap of the H-46 blade model show excellent correlation with experimental data.

2) Blade response characteristics are identified during low rotor speed regions of rotor run-up/run-down. One blade response characteristic suggests that aerodynamic forces are the main contributors to blade deformation while the other suggests that a transfer of system energy from kinetic to potential causes most of the blade deformation.

3) This study suggests that torsion is not required for rotorcraft with small amounts of pitch–flap coupling. Also, a quasi-steady aerodynamics model is sufficient for lower wind speeds; however, a higher fidelity aerodynamic model may be required for spatially varying gusts at higher wind speeds.

4) Under uniform WOD conditions, lateral cyclic and collective controls are shown to have a moderate impact on safe engagement envelopes.

5) The droop stop angle had a moderate effect on the tip deflections. This initial study does not suggest that droop stop angle changes would be an effective means to controlling the tunnel-strike phenomenon because of the delay in droop stop extension at higher droop stop angles. Ultimately, the droop stop could fail to extend, which would cause the blade to flap to the ground.

6) In the current flap stop configuration, a flap damper would not be effective in reducing the maximum downward tip deflections because of the small allowable flap hinge rotation. The present research suggests that a flap damper four times the strength of the H-46 lead/lag damper may be effective if the flap stop angle is raised.

7) During rotor engagement, only the ship-roll start position and amplitude had a large effect on maximum tip deflections. The largest tip deflections occur when the ship starts its motion tilted into or away from the wind for both small and moderate maximum roll amplitudes. The ship-roll period had no effect on maximum negative tip deflections.

Acknowledgments

This research was carried out with support from the U.S. Naval Air Warfare Center Aircraft Division at Patuxent River, Maryland. The Technical Monitors were Mark Whittle, Kurt Long, and Larry Trick. Support was also received from the Naval Aviation Depot at Cherry Point, North Carolina; the Technical Monitor was Robert Hellar. The authors are grateful

to George Thompson, William Harris, and John Kannon of Boeing Helicopters for providing technical information on the H-46 Sea Knight rotor system.

References

[1]Hurst, D. W., and Newman, S. J., "Wind Tunnel Measurements of Ship Induced Turbulence and the Prediction of Helicopter Rotor Blade Response," *Vertica*, Vol. 12, No. 3, 1988, pp. 267–278.

[2]Newman, S. J., "A Theoretical Model for Predicting the Blade Sailing Behaviour of a Semi-Rigid Rotor Helicopter," *Vertica*, Vol. 14, No. 4, 1990, pp. 531–544.

[3]Newman, S. J., "The Application of a Theoretical Blade Sailing Model to Predict the Behaviour of Articulated Helicopter Rotors," *Aeronautical Journal of the Royal Aeronautical Society*, Vol. 96, No. 956, 1992, pp. 233–239.

[4]Newman, S. J., "The Problems of Rotor Engagement and Disengagement of a Shipborne Helicopter," *Journal of Naval Sciences*, Vol. 20, No. 1, 1994, pp. 56–64.

[5]Newman, S. J., "The Verification of a Theoretical Helicopter Rotor Blade Sailing Method by Means of Windtunnel Testing," *Aeronautical Journal of the Royal Aeronautical Society*, Vol. 99, No. 982, 1995, pp. 41–51.

[6]Narveson, M. L., "Flow Modification over a Backward Facing Step," M.S. Thesis, Dept. of Aeronautical Engineering, U.S. Naval Postgraduate School, Monterey, CA, Sept. 1990.

[7]Geyer, W. P., "Aeroelastic Analysis of Transient Blade Dynamics During Shipboard Engage/Disengage Operations," M.S. Thesis, Dept. of Aerospace Engineering, Pennsylvania State Univ., University Park, PA, Aug. 1995.

[8]Geyer, W. P., and Smith, E. C., "Aeroelastic Analysis of Transient Blade Dynamics During Shipboard Engage/Disengage Operations," *Proceedings of the 2nd International AHS Aeromechanics Specialists' Meeting* (Fairfield County, CT), American Helicopter Society, Alexandria, VA, 1995, pp. 8-91–8-114.

[9]Geyer, W. P., Smith, E. C., and Keller, J., "Validation and Application of a Transient Aeroelastic Analysis for Shipboard Engage/Disengage Operations," *Proceedings of the 52nd Annual National Forum of the American Helicopter Society* (Washington, DC), American Helicopter Society, Alexandria, VA, 1996, pp. 152–167.

[10]Lemont, H. E., "Rotor Blade Flapping Control Mechanism," Patent no. 2,946,391, U.S. Patent Office, Filed Dec. 29, 1955, Patented July 26, 1960, Washington, DC.

[11]Ferrier, B., and Semenza, J., "NATC Manned Flight Simulator VTOL Ship Motion Simulation and Application," *Proceedings of the 46th Annual National Forum of the American Helicopter Society* (Washington, DC), American Helicopter Society, Alexandria, VA, 1990.

[12]Johnson, W., *Helicopter Theory*, Dover, New York, 1994.

[13]Bir, G., and Chopra, I., *University of Maryland Advanced Rotorcraft Code (UMARC) Theory Manual*, Univ. of Maryland, UM-AERO92-02, College Park, MD, Aug. 1992.

[14]Beddoes, T. S., and Leishman, J. G., "A Semi-Empirical Model for Dynamic Stall," *Journal of the American Helicopter Society*, Vol. 34, No. 3, 1989, pp. 3–17.

[15]Leishman, J. G., *Unsteady Aerodynamic Theory Manual for the Technology Complex (TC) Airloads and Induced Velocity CPCI of the Second Generation Comprehensive Helicopter Analysis (2GCHAS)*, Univ. of Maryland, UM-AERO90-30, College Park, MD, July 1990.